Large-Scale Patterns and Variability of Snowmelt and Parameterized Surface Albedo in the Arctic Basin

DAVID A. ROBINSON

Department of Geography, Rutgers University, New Brunswick, New Jersey

MARK C. SERREZE, ROGER G. BARRY, GREG SCHARFEN

Cooperative Institute for Research in Environmental Sciences, University of Colorado, Boulder, Colorado

GEORGE KUKLA

Lamont–Doherty Geological Observatory of Columbia University, Palisades, New York

(Manuscript received 30 May 1990, in final form 22 July 1991)

ABSTRACT

Visible-band satellite imagery is used to manually map surface brightness changes over sea ice throughout the Arctic Basin from May to mid-August over a 10-yr period. These brightness changes are primarily due to snowmelt atop the ice cover. Using image processor techniques, parameterized albedos are estimated for each brightness class. Snowmelt begins in May in the marginal seas, progressing northward with time, finally commencing near the pole in late June. Large year-to-year differences are found in the timing of melt, exceeding one month in some regions. Parameterized albedo for most regions of the pack ice exceeds 0.70 during May, declines rapidly during June, and reaches a seasonal low of between 0.40 and 0.50 by late July. For August, regional albedos, which also include areas of open water beyond the southern pack ice limit, are up to 0.16 lower than the corresponding values for pack ice areas only.

1. Introduction

By influencing surface albedo, variations in snowmelt atop the Arctic pack ice cover may be important forcing factors of northern high-latitude climates, with implications for the long-term mass balance and stability of the pack ice, and potential impacts on other parts of the Northern Hemisphere (Fletcher 1966; Barry 1983). Through the temperature–albedo feedback process, the Arctic may also be sensitive to perturbations resulting from increasing greenhouse gas concentrations. Continued monitoring of Arctic snow and ice cover is consequently an important component of the "early detection" strategy for identifying global and regional climate changes (Barry 1985).

Previous studies of snowmelt and albedo in the Arctic Basin, although numerous, have been of limited spatial and temporal scope, based largely on observations at drifting stations, on fast ice, and during aircraft missions (e.g., Laktionov 1953; Hanson 1961; Zubov 1963; Langleben 1971; Kuznetsov and Timerev 1973; Pautzke and Hornof 1978; Hanson 1980; Wen et al. 1980; Lapp 1982; Grenfell and Perovich 1984; Holt and Digby 1985; Grenfell and Lohanick 1985). Others have used these measurements (e.g., Larsson and Orvig 1962; Posey and Clapp 1964; Marshunova and Chernigovskiy 1966; Hummel and Reck 1979; Kukla and Robinson 1980; Robock 1980) and satellite passive microwave data (Carsey 1985) to estimate regional summer albedos. While viable techniques for routine automated extraction of surface albedo data from digital satellite imagery have been reported (e.g., Rossow et al. 1989), difficulties in routine automated identification of cloud cover over snow–ice surfaces (cf. Key and Barry 1989) and practical problems (in terms of cost and data storage) of digital processing of thousands of individual images have so far precluded efforts to produce a long-term database.

The recognized need for a long-term database led us to initiate a project to map patterns of snowmelt over the entire sea-ice cover of the Arctic Ocean (Fig. 1) by charting surface brightness changes through manual analysis of visible-band satellite imagery. Brightness classes were converted to parameterized surface albedo using image processor techniques. Initial results, based on two and four seasons of data, are discussed in Robinson et al. (1986, 1987) and Scharfen et al. (1987). The database has now been extended to ten spring and summer seasons. Although based on relatively simple techniques and parameterizations, and

Corresponding author address: Dr. Mark C. Serreze, CIRES, University of Colorado, P.O. Box 449, Boulder, CO 80309-0449.

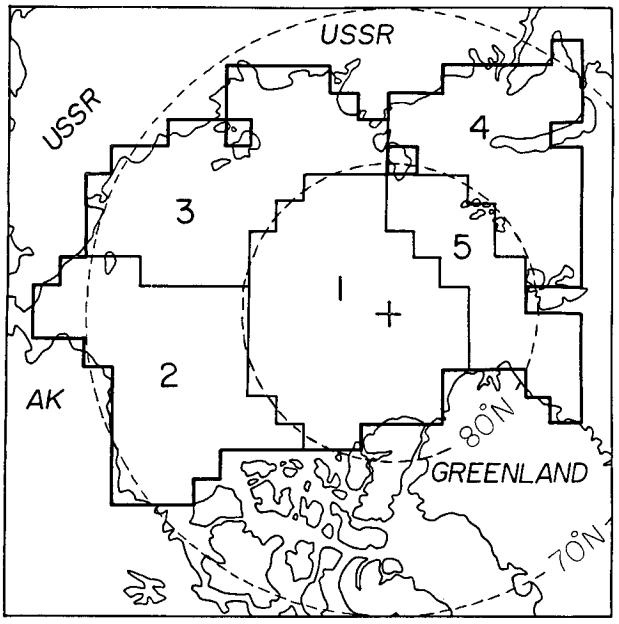

FIG. 1. Arctic Basin study area comprising 223 grid cells. Cells are combined to define five subregions: 1) central Arctic, 2) Beaufort/Chukchi seas, 3) east Siberian/Laptev seas, 4) Kara/Barents seas, and 5) northwest North Atlantic.

lacking strict radiometric control, our database represents the first available source of information on climatological characteristics of large-scale patterns of snowmelt and surface albedo over the entire Arctic Basin. The present paper details the analysis procedure and results from the 10-season database.

2. Data and methods

a. Satellite imagery

Images from the U.S. Air Force Defense Meteorological Satellite Program (DMSP) near-polar orbiter served as the primary data source. These images are archived as transparencies only, produced operationally from digital data in a broadband channel in the visible and near-infrared (0.4–1.1 micrometer) wavelengths. The DMSP satellites have an orbital period of approximately 102 min, inclined 98.7° to the equator, with each orbital pass approximately 25.4° west of the preceding one. Satellites are equipped with an Operational Linescan System, scanning 13° to either side of nadir, with a scan-angle corrected field of view of approximately 0.6 km. Approximately 85% of all DMSP images used were orbital-swath format. These images provide daily Arcticwide coverage at a degraded resolution of about 2.7 km. DMSP images with local coverage at the 0.6-km resolution, available for the Beaufort and Chukchi seas only (Fig. 1), and NOAA Very High Resolution Radiometer (VHRR) and Advanced VHRR (AVHRR) 1.1-km resolution visible-band images were used when the 2.7-km DMSP products were missing from the archive or were of poor quality. Selected 80-m resolution Landsat Multispectral Scanner (MSS) visible-band scenes (hard copy) were used for comparisons with the DMSP and AVHRR imagery.

b. Identification of melt over sea ice

Snowmelt during spring and summer is the primary cause of large-scale changes in the brightness of the sea-ice cover observed in visible-band satellite imagery. As the overlying winter snow cover ripens and begins to melt, there is a progressive decrease in surface brightness as well as characteristic changes in surface texture. This is a result of snow becoming wet and decreasing in depth, as well as due to the formation of meltponds and exposure of bare ice (Barry 1983). The surface may first appear mottled, eventually becoming more uniformly gray in appearance as the snow dissipates and meltponds drain. After drainage of meltponds, the surface may again brighten, particularly over fast ice (largely undeformed coastal ice locked to the shoreline) and first-year pack ice (pack ice that forms and melts in a single year) (Zubov 1963; Jacobs et al. 1975; Lapp 1982; Holt and Digby 1985). While individual meltponds and details of the snow cover are not resolved in the DMSP and AVHRR imagery, comparisons with coincident 80-m resolution Landsat imagery indicate that the areally integrated appearance of melt features can be readily recognized in the lower-resolution DMSP and AVHRR products (Scharfen et al. 1987).

Using the DMSP and AVHRR images, four surface brightness classes were manually charted over the pack-ice cover for 3-day periods from May to mid-August for the years 1975, 1977–80, and 1984–88. Sufficient images were not available for intervening years. Review of the literature cited in the Introduction indicates that our brightness class 1 corresponds to fresh snow cover over 95% of the ice. Class 2 is found when snow covers between 50% and 95% of the surface, with the remainder being bare or ponded ice. In spring this is considered to be the initial stage of snowmelt. Class 3 represents the advanced to final stage of snowmelt, with numerous meltponds and between 10% and 50% of the ice surface snow covered, or, following pond drainage, predominantly bare ice (Fig. 2). Field studies (e.g., Kuznetzov and Timerev 1973; Hanson 1980) indicate that meltponds are typically extensive for the first two to three weeks that class 3 is observed. Heavily ponded or flooded ice is represented by class 4, generally limited to regions of fast ice near outlets of major rivers along the Siberian Arctic coast.

Typically 15–25 images were used during each charting interval. The 3-day charting interval was usually found to be long enough to obtain at least one clear-sky image over a given area, yet short enough to permit evaluation of temporal and regional variations

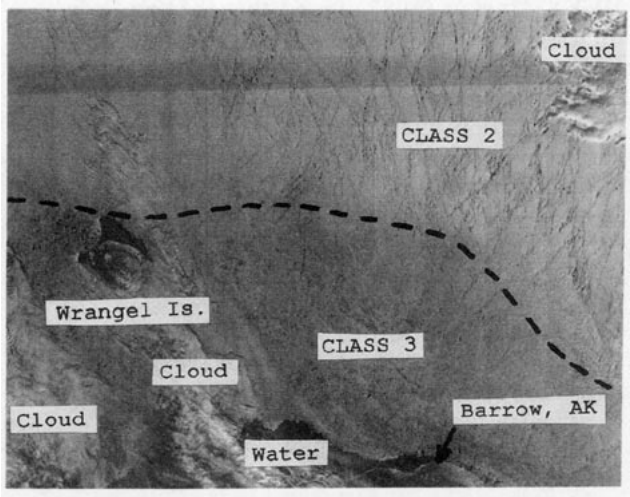

FIG. 2. High-resolution (0.6-km) DMSP shortwave image of the Beaufort and Chukchi seas for 16 June 1978, illustrating stages of snowmelt on the sea ice. The lower half of the image shows brightness class 3, while the upper half (north) shows brightness class 2. The border between the two classes is indicated by the dotted line. The horizontal band across the top of the image is caused by a satellite data-processing problem.

in surface brightness. Surface–cloud discrimination was based on identification of cloud shadows, cloud motion, and characteristic features of the surface, including ice floes, leads, and meltponds (Robinson et al. 1985; Serreze and Rehder 1990). Extensive cloud cover and poor lighting precluded charting after mid-August.

Consistent with the aim of interpreting brightness changes as due to snowmelt, efforts were made to map what appears to be the snow–ice surface only, ignoring large, visible leads (linear openings in the pack-ice cover) and polynyas (broad openings). Although smaller features can be detected in the higher-resolution 0.6-km DMSP and 1.1-km VHRR and AVHRR products, comparisons with coincident 2.7-km DMSP images show no systematic tendency to chart a higher or lower brightness class when these images are used. Nevertheless, regardless of image type, as snow melts and image contrast decreases, the size of features that cannot be detected increases.

Even high concentration ice, however, contains dark, undetectable features that reduce pixel brightness. We assume that at least during early May, such features (as well as detectable features ignored during charting) could be snow-free thin ice or a mixture of thin ice and open water in newly opened leads. Such effects on pixel brightness will tend to increase during summer as thin ice melts and the true open-water fraction increases. This should be most significant in the marginal ice zone (MIZ), where ice concentrations are characteristically low. Despite snowmelt being the dominant factor influencing surface brightness, the presence of open water within the pack ice necessitates assumptions in our parameterization and interpretation of surface albedo (see later discussion).

Because of the relatively small solar zenith angles of the Arctic summer and at the satellite viewing time and angle, specular reflection is minimal over snow, ice, and water surfaces (Taylor and Stowe 1984). This and other potential effects on surface brightness, such as shadowing in areas of ridged ice, particulates in the overlying snow cover and Arctic haze, are not considered to influence significantly the brightness class interpretations.

c. *Digitization of data*

The surface brightness maps were digitized to the Limited-Area Fine Mesh version of the U.S. National Meteorological Center (NMC) grid, dividing the study area into 223 cells (Fig. 1). Grid cells were simply assigned the value of the predominant melt class in that cell. Open-water cells were defined using the Navy/NOAA Joint Ice Center ice concentration chart (based primarily on satellite data; see Godin 1981) closest in time to the analyzed 3-day interval, digitized to the same NMC grid. Since these charts are produced at weekly intervals, typically two brightness charts are assigned the same open-water grid cells. Generally, 20% of all ice-covered cells were initially missing from each chart (primarily due to cloud cover). In order to minimize the number of missing cells without resorting to spatial interpolation, cells with missing data were assigned the values of corresponding cells from the immediately preceding chart (if available). If still missing, and corresponding cells from the immediately subsequent chart had a nonmissing value, the cells were assigned that value. By these techniques, data were usually available over more than 90% of all cells for each chart.

d. *Parameterization of surface albedo*

Parameterized albedos were next assigned to each grid cell. Using an image processor, digital numbers (DNs) were measured for targets of sea ice and open water within rectangular regions of approximately 9000 km^2 from clear-sky portions of 20 redigitized DMSP images, covering May through July for 1977 and 1979. Both the 0.6-km and 2.7-km DMSP products were used. A total of 158 rectangular regions were examined, with approximately 1400 DN values obtained for each region. Mean DNs were then obtained for these regions. The highest and lowest mean DN values of snow-covered sea ice and open water, respectively, were then used as tie points, and assigned clear-sky albedos, based on measured ground and aerial data (e.g., Hanson 1961; Nazintsev 1964; Langleben 1971; Bryazgin and Koptev 1970; Payne 1972; Grenfell and Maykut 1977; Pautzke and Hornof 1978; Cogley 1979). On the basis of these data, the upper tie-point brightness was as-

signed an albedo of 0.79 until late June, after which a value of 0.69 was used due to the decrease in maximum image brightness associated with snowmelt. Our open-water albedo was taken as 0.12 (Payne 1972; Cogley 1979). The literature values of albedo (and hence our resultant values) refer to the integrated solar spectral range of approximately 0.3–2.7 μm.

The average DNs from regions corresponding to the charted classes were then converted into clear-sky albedos by linear interpolation between the tie points. The resulting mean clear-sky values were 0.75 (class 1), 0.59 (class 2), 0.44 (class 3), and 0.27 (class 4), with standard deviations of 0.04 (class 1), 0.07 (class 2), 0.08 (class 3), and 0.05 (class 4). These are the same values used in our previous work (e.g., Scharfen et al. 1987). The means for classes 2 and 3 are similar to those reported from aircraft studies by Buzuev et al. (1965) for corresponding surface conditions. The aforementioned procedure has been used previously (e.g., Preuss and Geleyn 1980; Robinson and Kukla 1985) and is well suited for use with the broadband DMSP imagery (Shine and Henderson-Sellers 1984).

Cloud cover tends to increase albedo due to preferential absorption of near-infrared radiation by clouds. In consideration of this effect, the clear-sky albedos were adjusted by +0.05 for brightness classes 1–3 and +0.02 for class 4, based on published data (Buzuev et al. 1965; Kuznetsov and Timerev 1973; Gorshkov 1983; Grenfell and Perovich 1984), with a constant 75% cloud cover assumed for each grid cell (Kukla and Robinson 1988). We will return to this assumption shortly. With the cloud cover adjustments, the final adopted class values used here are 0.80 (class 1), 0.64 (class 2), 0.49 (class 3), and 0.29 (class 4), with the same standard deviations as for the clear-sky values.

These class albedos are considered to be weighted by open water in the pack ice. Using submarine sonar data, Key and Peckham (1991) find that lead distributions tend to follow a negative-exponential distribution, such that the majority of open water in the pack ice is attributed to small leads. For example, if we assume a mean lead width of 100 m (which is probably unrealistically large), then 99.3% of the leads are <500 m in width. A 500-m lead should be near the detection limit of the 2.7-km DMSP imagery (comprising 85% of all images used) under conditions of high image contrast. Consequently, the bulk of open-water features in typical pack ice should be subresolution and hence included in our albedo estimates. The effects of undetected areas of dark, new thin ice will also be included in these estimates.

A first-order assessment of the effects of undetectable open water versus melt on our class albedos can be obtained by assuming representative ice concentrations for spring and summer and linearly weighting the clear-sky class albedos using an open-water albedo of 0.12. From data collected in the northern Beaufort Sea during the Arctic Ice Dynamics Joint Experiment (AIDJEX), Maykut (1982) found that the areal coverage of ice in the 0–0.1-m thickness category was about 2% in May and 9% in July. Assuming that these values are reasonably representative of the undetectable open-water fraction in the interior pack ice, and applying the above technique, we find that during May, when class 1 brightness (clear-sky albedo = 0.75) is present over most of the pack-ice cover (see later discussion), weighting by 2% open water yields an ice-only albedo of 0.76. For July, when class 3 (clear-sky albedo = 0.44) is usually predominant (see later discussion), the 9% open-water fraction yields an ice-only albedo of 0.47. In both cases, the difference between the concentration-weighted and ice-only value is small, and the resulting seasonal decline in albedo of 0.29 for the ice-only values (which can be considered due to surface melt alone) is within 0.02 of the concentration-weighted change.

Although ice concentrations as low as 60% have been observed locally in the northern Beaufort Sea during late summer (Serreze et al. 1990), the effects of ice concentration from May through mid-August are likely to be substantial only in the MIZ. The MIZ, defined here as areas where the JIC charts show concentrations < 75%, typically represents less than 10% of the sea-ice cover through the melt season. From here on, the term "pack ice" will refer to those areas defined by the JIC charts as having >10% ice cover, with grid cells less than this concentration value considered to be open water.

Our albedo data are only appropriate for broad climatological analysis. First, each melt class corresponds to a broad range in albedo. Second, while in support of our simple treatment of cloud cover, monthly maps for summer by Gorshkov (1983) and Serreze and Rehder (1990) show little spatial variation in cloud cover over most of the pack ice (primarily low-level Arctic stratus; see Herman and Goody 1976), there can be large interannual and short-term variability (Barry et al. 1987; Serreze and Rehder 1990; Robinson et al. 1985). Third, since the effects of large, visible leads and polynyas were excluded during charting, our regional albedos will tend to be slightly high. We also take no account of spatial or temporal variations in these features. In consideration, we restrict our analysis of albedo to mean results over the 10-yr record.

3. Results

a. Progression of snowmelt over pack ice

The year 1986 typifies the pattern of snowmelt atop the pack-ice cover found in most years (Figs. 3a–d). Melt begins in the marginal seas during May (Fig. 3a) and progresses poleward during June (Fig. 3b). The region surrounding the pole is the last to melt, with class 2 persisting into July (Fig. 3c). By August (Fig. 3d) snow cover in most years is completely removed over the entire pack-ice cover. The progression of sur-

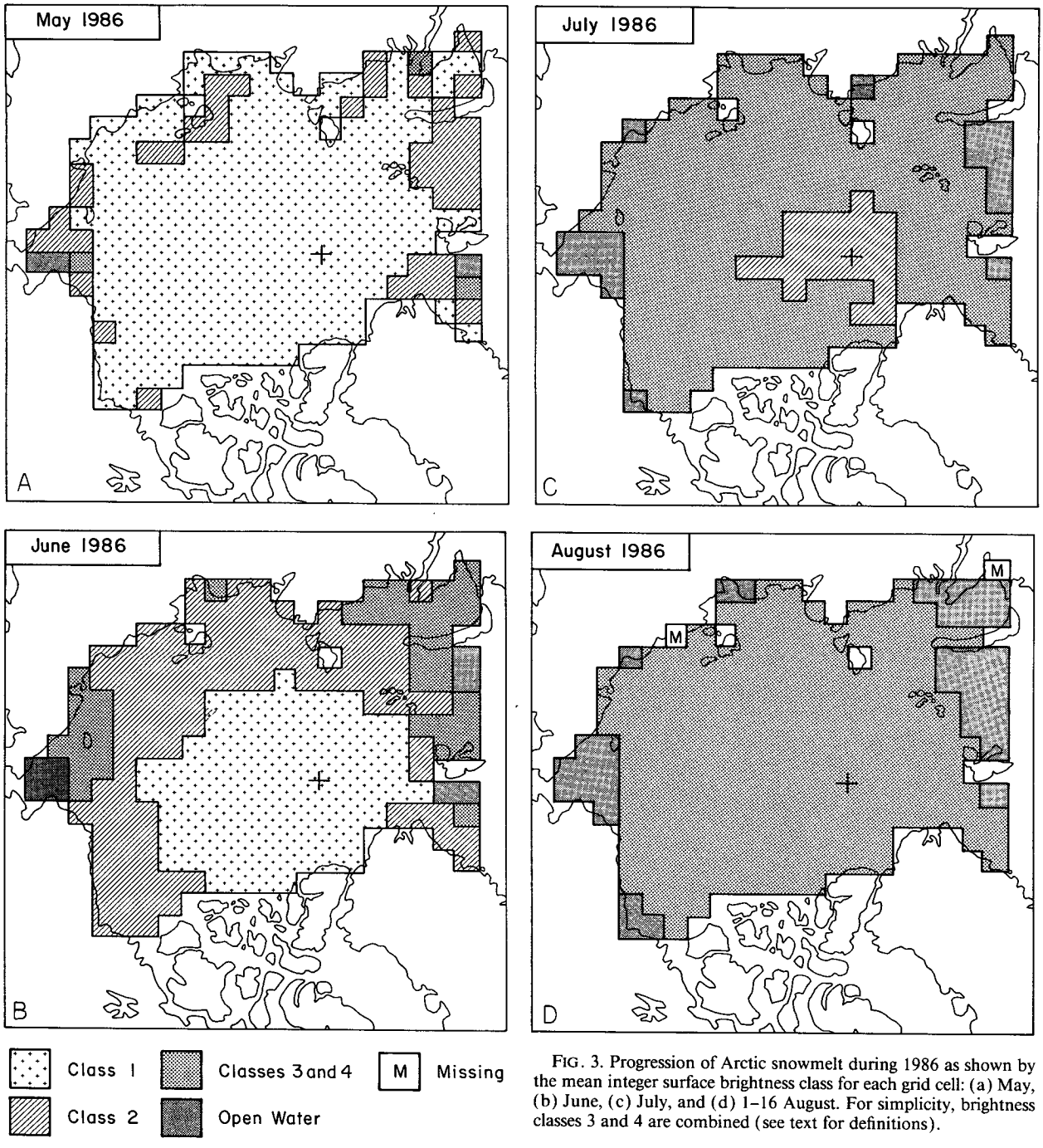

FIG. 3. Progression of Arctic snowmelt during 1986 as shown by the mean integer surface brightness class for each grid cell: (a) May, (b) June, (c) July, and (d) 1–16 August. For simplicity, brightness classes 3 and 4 are combined (see text for definitions).

face melt is accompanied by an asymmetrical retreat of the ice edge northward. In this regard, however, 1986 is somewhat atypical in that ice remained fairly extensive throughout the summer. This contrasts with 1977, when by the middle of August, open water was present over nearly the entire length of the Eurasian coast.

To examine year-to-year variations in regional snowmelt, data were stratified by the regions shown in Fig. 1. Dates for the onset of melt were determined in each of these regions for each year, defined by the date when at least 50% of all nonwater cells in a region were class 2 or greater (Table 1). The regional date of advanced melt was similarly defined as the date when at least 50% of all nonwater cells in a region were class 3 or greater (Table 2). As persistent cloud cover sometimes precluded charting over part of a region for a

TABLE 1. Date of melt onset by region and year, ranked from the earliest to latest date. Ties are indicated by a T to the left of the rank numbers. Mean dates based on all data and the range in dates (days) between extreme years are also given.

	Central Arctic		Beaufort/Chukchi		Laptev/E. Siberian		Kara/Barents		NW North Atlantic	
Year	Rank	Date	Rank	Date	Rank	Date	Rank	Date	Rank	Date
1975	10	7/8	9	6/14	10	6/29	T3	5/12	7	6/8
1977	1	6/5	3	5/21	1	5/21	T3	5/12	2	5/12
1978	6	6/23	4	5/24	3	6/8	7	5/18	4	5/24
1979	7	6/29	10	6/20	T7	6/17	9	5/30	6	6/2
1980	8	7/2	T7	6/11	9	6/23	6	5/15	8	6/23
1984	T3	6/14	T1	5/9	4	6/11	1	5/3	1	5/6
1985	5	6/20	6	6/8	T5	6/14	8	5/27	5	5/27
1986	9	7/5	T7	6/11	T5	6/14	2	5/6	—	—
1987	2	6/11	5	5/30	2	6/5	T3	5/12	3	5/18
1988	T3	6/14	T1	5/9	T7	6/17	—	—	—	—
Mean		6/23		5/30		6/14		5/15		5/27
Range		27 d		42 d		39 d		24 d		48 d

given 3-day mapping interval, dates for each region were calculated using three criteria: 1) that a given chart met the 50% class threshold with >33% of the possible (nonwater) cells having data; 2) same as 1) except with >50% of the possible cells having data; and 3) same as 1) except >67% of possible cells having data. If the range in dates found by these three criteria differed by more than two charts (6 days), the respective date for that year was considered unreliable and discarded. Otherwise, the three dates were averaged.

In examining the mean values and ranges given in Table 1, it is seen that the onset of melt usually takes place first during mid-May in the Kara and Barents seas, followed in late May by the northwest North Atlantic and the Beaufort and Chukchi seas. It begins in mid-June over the east Siberian and Laptev seas, followed about a week later by the central Arctic. This is in accord with results presented in Fig. 3. The range between extreme years, however, is quite large, being from 24 days in the Kara/Barents seas region to as much as 48 days in the northwest North Atlantic, suggestive of large year-to-year variability in atmospheric forcings controlling the melt process. Results for individual years show that in the central Arctic, melt occurred earliest in 1977 (5 June) and latest in 1975 (8 July). Years of early melt in the marginal seas include 1977, 1984, and 1988. Late melt occurred in 1975, 1979, and 1980, with dates ranging between 30 May and 29 June. By summing the individual rankings across the regions for each year, and using only years for which the regional date of melt onset is defined, basinwide snowmelt occurred earliest in 1977 and 1984 and latest in 1975 and 1979.

The stage of advanced-to-final melt (Table 2) starts about one month after melt onset in the northwest North Atlantic, Kara/Barents, and Beaufort/Chukchi

TABLE 2. Date of advanced melt by region and year, ranked from the earliest to latest date. Ties are indicated by a T to the left of the rank numbers. Mean dates based on all data and the range in dates (days) between extreme years are also given.

	Central Arctic		Beaufort/Chukchi		Laptev/E. Siberian		Kara/Barents		NW North Atlantic	
Year	Rank	Date	Rank	Date	Rank	Date	Rank	Date	Rank	Date
1975	T3	7/8	—	—	10	6/29	4	6/17	T3	6/29
1977	T1	7/2	1	6/11	T3	6/20	T1	6/2	2	6/23
1978	T6	7/11	T8	7/2	T7	6/23	9	6/29	4	6/29
1979	T6	7/11	T6	6/26	T7	6/23	8	6/23	T3	6/29
1980	T6	7/11	5	6/23	T7	6/23	T5	6/20	8	7/8
1984	9	7/26	2	6/17	T3	6/20	T5	6/20	—	—
1985	10	7/29	T8	7/2	T3	6/20	T5	6/20	6	6/29
1986	T3	7/8	T6	6/26	T3	6/20	3	6/11	7	7/5
1987	T1	7/2	T3	6/20	1	6/14	T1	6/2	1	6/17
1988	T3	7/8	T3	6/20	2	6/17	—	—	—	—
Mean		7/11		6/23		6/20		6/17		6/29
Range		27 d		21 d		15 d		27 d		21 d

regions, about three weeks later in the central Arctic, but only one week later in the east Siberian/Laptev region. The latter region is hence analogous to the polar tundra in exhibiting a rapid removal of the snow cover (Holmgren et al. 1975; Robinson 1986). The Laptev Sea is a major entrance zone for summer cyclones migrating into the Arctic Basin (Serreze and Barry 1988), suggesting control by advection of warm air masses. In the central Arctic the range among extreme years in the timing of advanced melt is the same as for the onset of melt (27 days). It is slightly larger for the Kara/Barents seas, but much less in the remaining regions. The advanced stage of melt for the central Arctic occurred earliest in 1977 and 1987 (2 July) and latest in 1985 (29 July). Early dates of advanced melt in the marginal seas occurred in 1977 and 1987; late years include 1975, 1978, 1980, and 1985. By summing regional rankings as before, advanced melt over the entire pack ice was earliest in 1987, followed closely by 1977, and latest in 1978.

The final stage of snowmelt (class 3 or 4) was achieved over all grid cells in the study area in all summers except 1984 and 1985. In 1984 class 2 covered at least 12% of the basin in mid- and late summer and remained above 4% in 1985. New snow also temporarily covered the ice in scattered portions of the basin during several summers (e.g., 1979), tending to become more common and persistent in the central Arctic by mid-August.

b. Surface albedo

Figure 4 shows the mean basinwide progression of parameterized surface albedo for pack-ice cells only (those with >10% ice cover). Individual charts were only considered when at least 50% of the 223 possible available cells had valid data. Based on the ten years of data, albedo during May decreases slowly from the high of nearly 0.80 to the middle 0.70s. The month as a whole has a long-term mean value of 0.77. June begins with a long-term mean value of about 0.72, dropping to 0.53 by the end of the month. The monthly mean albedo is 0.66.

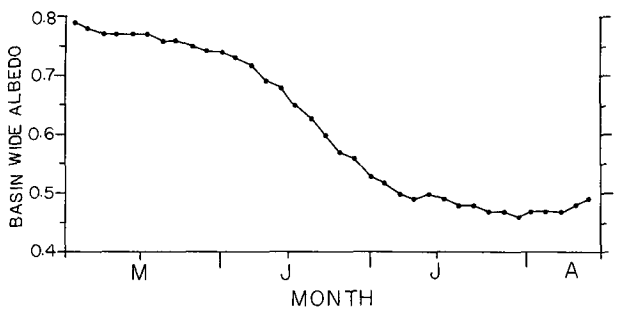

FIG. 4. Basinwide mean surface albedo of the pack-ice cover in 3-day increments between 1–3 May and 14–16 August over the ten study years for pack-ice cells (>10% ice cover). Results are based on charts with data for at least 50% of all grid cells.

TABLE 3. Long-term monthly means (August values for first half of month only) of parameterized regional surface albedo for pack-ice cells (>10% ice cover). Regions are shown in Fig. 1. Values in parentheses are the 10-yr mean JIC ice concentrations for pack-ice cells.

	Central Arctic	Beaufort/ Chukchi	Laptev/E. Siberian	Kara/ Barents	NW North Atlantic
MAY	0.80 (95)	0.76 (95)	0.78 (95)	0.72 (93)	0.75 (94)
JUN	0.74 (95)	0.64 (94)	0.63 (94)	0.58 (90)	0.65 (94)
JUL	0.54 (95)	0.49 (93)	0.46 (91)	0.43 (78)	0.49 (92)
AUG	0.51 (95)	0.48 (92)	0.44 (84)	0.39 (69)	0.47 (89)

During July the pack-ice albedo declines at a slower rate than in June, indicating that most of the snow cover is removed from the sea ice by this time. The curve bottoms out in late July, with a seasonal low of 0.46 occurring near the end of the month. The 10-yr mean monthly July albedo is 0.49. Little additional change is seen in basinwide pack-ice albedo until the middle of August, when values begin to rise in response to accumulation of new snow over the central Arctic. The 10-yr mean for the first half of August is 0.47.

Table 3 gives a regional breakdown of parameterized monthly mean surface albedo for pack-ice cells. Results for each region are based on charts having valid data for at least 50% of all possible nonwater cells in that region. Ten-year mean ice concentrations for ice-covered cells, calculated from the weekly JIC analyses, are also listed in Table 3 to present some idea of regional variability in the open-water fraction. For the interior pack ice, the JIC tends to simply report concentrations as 100% or in a single broad category of 90%–100%. We suspect that the mean JIC values listed in Table 3 for the central Arctic are slightly low for spring and slightly high for late summer.

As seen from Table 3, the 10-yr mean pack-ice albedo in all regions exceeds 0.70 for May. June shows large regional differences in parameterized pack-ice albedo. Although the mean albedo of the central Arctic remains high (0.74), it is now as low as 0.58 in the Kara/Barents seas region. July shows a continued decrease in pack-ice albedo for all regions. The central Arctic mean remains highest (0.54), with the lowest value of 0.43 again found for the Kara/Barents seas. Albedos are lowest during August, with only the central Arctic remaining above 0.50. As in previous months, albedo is lowest for the Kara/Barents seas, with a mean value of 0.39.

Table 4 shows monthly mean regional albedos computed in the same manner as those for Table 3, except that open-water cells (those with <10% ice cover) with an assumed albedo of 0.12 are included. The average percent of each region represented by open-water cells is also shown. Since open-water cells were never found

TABLE 4. Long-term monthly means (August values for first half of month only) of parameterized regional surface albedo based on both pack-ice cells (>10% ice cover) and open-water cells (<10% ice cover). Values in parentheses are the mean percent of the region represented by open-water cells. Regions are shown in Fig. 1.

	Beaufort/ Chukchi	Laptev/E. Siberian	Kara/ Barents	NW North Atlantic
MAY	0.76 (0)	0.78 (0)	0.70 (3)	0.71 (6)
JUN	0.62 (3)	0.62 (1)	0.55 (8)	0.62 (6)
JUL	0.44 (14)	0.44 (5)	0.34 (30)	0.47 (6)
AUG	0.39 (25)	0.38 (18)	0.23 (60)	0.44 (10)

in the central Arctic region, results for this region are the same as in Table 3 and are not shown. As can be seen, the 10-yr mean "all surface" albedos (Table 3) remain within 0.04 of the pack-ice values for all months in the northwest North Atlantic sector but are from 0.06–0.16 lower by August in the Beaufort/Chukchi, Laptev/East Siberian, and Kara/Barents sectors, due to retreat of the ice front in these regions.

Results from the basinwide and regional analyses are summarized in Figs. 5a–d by maps of mean monthly parameterized albedo in which all data, including open-water cells, are included. The map for May (Fig. 5a) shows a broad region surrounding the Pole where albedo is at its maximum parameterized value of 0.80. Albedo is over 0.75 for most of the pack ice. A sharp decrease is noted in the northwest North Atlantic sector and the southern Beaufort Sea due to snowmelt, open-water cells, and cells with low concentration ice. June (Fig. 5b) shows a roughly symmetric pattern, with albedo decreasing from near the pole southward, corresponding to the typical pattern of snowmelt shown in Fig. 3. Values are still in excess of 0.75 near the pole. As with May, sharp reductions in albedo are shown for the marginal seas. July and August (Figs. 5c,d) show similar patterns, but with lower albedos. Values remain above 0.50 near the pole, even in August.

4. Discussion

The spatial progression of snowmelt identified in this study compares favorably with the summary of surface melt prepared by Marshunova and Chernigovskiy (1978), which shows a concentric pattern of melt over the Arctic pack ice progressing toward the pole by early July. From a study of sequential passive microwave satellite data for 1974, Campbell et al. (1980) suggested that melt begins along the Siberian coast in May and moves as a roughly linear front across the pole, reaching the Canadian and Greenland coasts about a month later. Reexamination of their data by Crane et al. (1982) indicates that the color coding of the microwave imagery yielded a spurious impression of the progressing melt front. Our results confirm Crane's view.

Previous estimates of July surface albedo for the interior basin range from 0.40 (Robock 1980) to 0.65 (Hummel and Reck 1979). Our central Arctic value of 0.54 falls in the middle of this range. Carsey (1985) used microwave satellite data to estimate surface albedo indirectly by estimating the areal coverage of bare ice from the microwave data and the coverage of meltponds and leads from published reports. Parameterized albedos were then assigned to each surface type and weighted according to their coverage. The inner basin albedo for mid-July 1974 was estimated to be 0.58, in good agreement with our central Arctic values. While in the present paper we restrict our analysis of albedo to mean results over the ten years of data, Rossow et al. (1989) compared our July 1977 albedos (see Scharfen et al. 1987) with those derived for the same time using digital data from the NOAA-5 scanning radiometer and found mean monthly regional values in disagreement by only 0.02 to 0.07. Ross and Walsh (1987) also compared our earlier results for 1977 and 1979 (Scharfen et al. 1979) with albedos derived from the Hibler (1979) sea-ice model with an improved albedo parameterization and reproduced the lower albedos calculated for the earlier year as well as regional differences.

Variations in the timing of surface melt and of parameterized albedo should show associations with large-scale atmospheric forcings. For example, our monthly mean maps of parameterized albedo (Fig. 5a–d) agree well with patterns of cumulative melting degree days over the Arctic Ocean (not shown) calculated from drifting buoy temperature data for 1979–86 (e.g., Thorndike and Colony 1980). Compared to 1979, melt was very early during 1977 (Tables 1 and 2). Basinwide average temperatures compiled by Hansen et al. (1983), cited by Ross and Walsh (1987), indicate that summer temperatures were 1°–2.5°C higher in 1977 than in 1979.

One important aspect that needs to be addressed further is the role of cloud cover on the timing of melt. As discussed earlier, since cloud cover tends to absorb preferentially in the near infrared, surface albedos tend to be higher when skies are cloudy. Nevertheless, it has often been observed (e.g., Ambach 1974) that under conditions of high albedo and low solar flux (i.e., spring), surface net radiation tends to increase when cloud cover is present, due to the increase in the downwelling longwave component.

Estimates compiled by Maykut (1986) indicate that surface net radiation over the central Arctic first turns positive during May at which time cloud cover also shows a sharp increase to approximately 70% (Huschke 1969). While solar radiation becomes important in May, part of the increase in net radiation may also be due to the effects of increased cloud cover. According to Untersteiner (1961), large-scale melt of the pack begins when low-level stratus begins to move into the area. However, we do not observe melt in this region

until at least early June (Table 1), suggesting that solar radiation plays a more important role. Consistent with this view, results from manual interpretation of cloud cover from satellite imagery by Kukla and Robinson (1988) show that the clear-sky fraction in June and July for the central Arctic was 12% and 10% greater, respectively, in 1977 than 1979. Melt occurred over three weeks earlier in the former year.

We are currently compiling a cloud-cover database for the Arctic Ocean, based on manual analysis of DMSP satellite imagery, for the same ten years for which we have snowmelt data. Analysis of these data should provide additional insight into the relationships between snowmelt and cloud cover.

5. Summary and conclusions

Our long-term database reveals a characteristic progression of snowmelt from the marginal seas toward the central Arctic. Melt typically commences in lower latitudes during May, reaching the pole by late June. The snow cover tends to be completely removed by

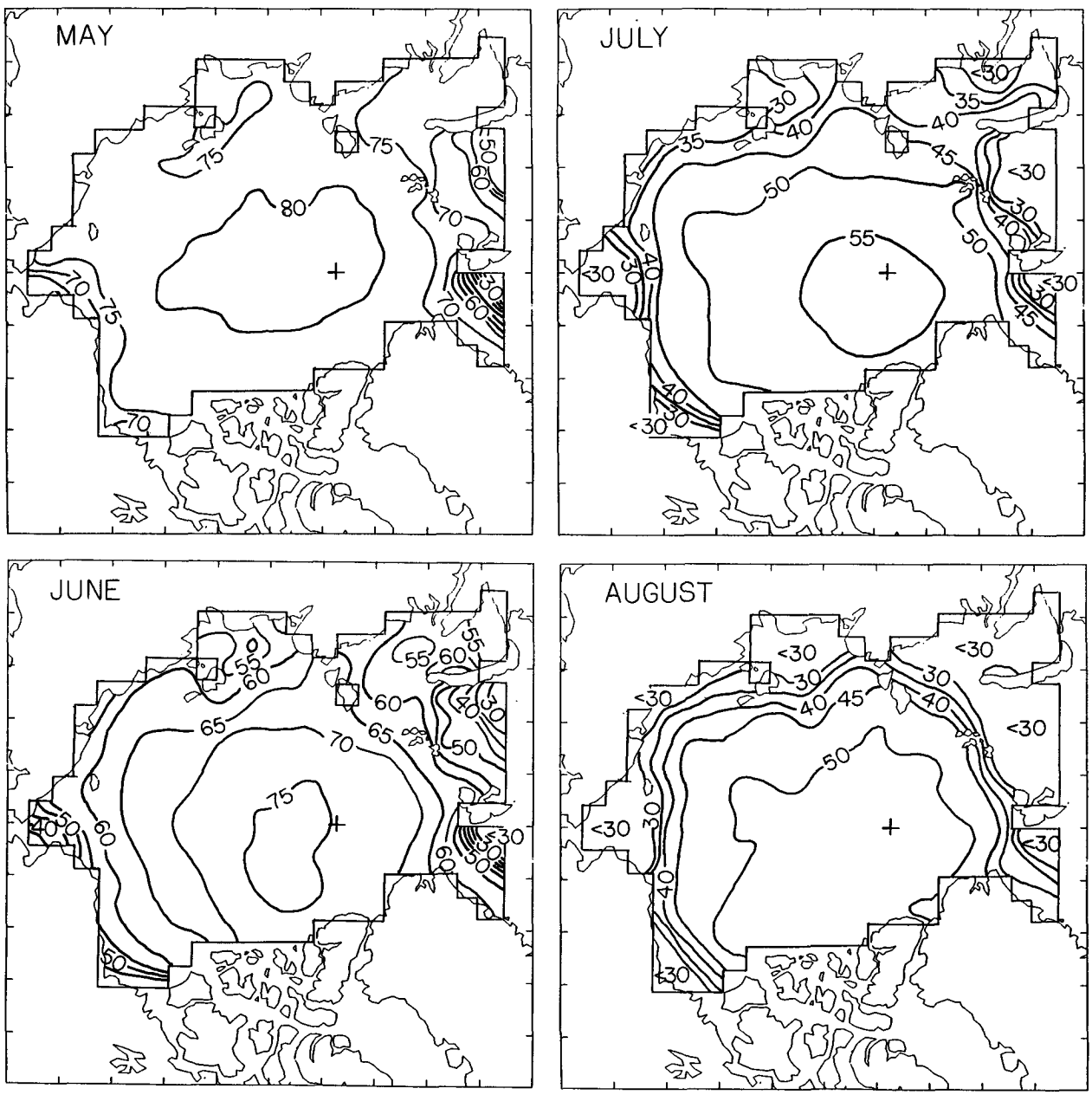

FIG. 5. Ten-year monthly mean surface albedos (expressed in %) within the Arctic study region for (a) May, (b) June, (c) July, and (d) the first half of August. Both pack-ice (>10% ice cover) and open-water (<10% ice cover) cells are included.

late July, with new snow cover occasionally found in the central Arctic by mid-August. Year-to-year differences in the timing of melt in excess of a month are observed.

Surface albedos derived from the surface melt analysis indicate that basinwide albedos of the pack-ice cover range between 0.70 and 0.80 in May, drop off rapidly during June, and reach a minimum of about 0.45 toward the end of July. By August, in most of the marginal seas, corresponding regional "all surface" albedos, which include open-water cells, are up to 0.16 lower than for pack-ice areas only.

Although our surface albedo database is founded on a simple parameterization, it represents the only available long-term, basinwide analysis suitable for use in modeling studies. Climate simulations with GCMs using these albedo values (cf. Morassutti 1989) may offer useful insight into the role of sea-ice variability on high-latitude climate sensitivity.

Acknowledgments. We thank M. Brown, W. Capehart, R. Henry, S. Innis, and D. Van Metre for participating in the construction of the melt charts and M. Neary for drafting. This work was supported by NSF Grant ATM 90-16563 and the Office of Naval Research University Research Initiative Contract N00014-86-K-0695.

REFERENCES

Ambach, W., 1974: The influence of cloudiness on the net radiation budget of a snow surface with high albedo. *J. Glaciol.*, **13,** 73–84.

Barry, R. G., 1983: Arctic Ocean ice and climate: Perspectives on a century of polar research. *Ann. Assoc. Amer. Geogr.*, **73,** 485–501.

——, 1985: The cryosphere and climate change. *Detecting the Climatic Effects of Increasing Carbon Dioxide,* M. MacCracken, F. Luther, Eds., DOE/ER-0235, U.S. Dept. Energy, 109–148.

——, R. G. Crane, A. Schweiger, and J. Newell, 1987: Arctic cloudiness in spring from satellite imagery. *J. Climatol.* **7,** 423–451.

——, M. W. Miles, R. C. Cianflone, G. Scharfen, and R. C. Schnell, 1989: Characteristics of Arctic sea ice from remote sensing data and their relationship to atmospheric processes. *Ann. Glaciol.*, **12,** 9–15.

Bryazgin, N. N., and A. P. Koptev, 1970: Spectral albedo of snow–ice cover. *Problems of the Arctic and Antarctic,* **31,** 79–83.

Buzuev, A. Ya., N. P. Shesterikov, and A. A. Timerev, 1965: Al'bedo l'da v arkticheskikh moryakh po dannym nablyudeniy s samoleta (Albedo of ice in Arctic seas from airborne observational data). *Problemy Arktiki i Antarktiki,* **20,** 49–54.

Campbell, W. J., R. O. Ramseier, H. J. Zwally, and P. Gloersen, 1980: Arctic sea ice variations from time-lapse passive microwave imagery. *Bound.-Layer Meteor.*, **18,** 99–106.

Carsey, F., 1985: Summer Arctic sea ice character from satellite microwave data. *J. Geophys. Res.*, **90,** 5015–5034.

Cogley, J. G., 1979: The albedo of water as a function of latitude. *Mon. Wea. Rev.*, **107,** 775–781.

Crane, R. G., R. G. Barry, and H. J. Zwally, 1982: Analysis of atmosphere–sea ice interaction in the Arctic basin using ESMR microwave data. *Int. J. Remote Sens.*, **3,** 259–276.

Fletcher, J. O., 1966: The arctic heat budget and atmospheric circulation. *Proc. Symp. Arctic Heat Budget and Atmospheric Circulation,* J. O. Fletcher, Ed., Mem. RM-5233-NSF, Rand Corp, 23–43.

Godin, R. H., 1981: Sea ice charts of the Navy/NOAA Joint Ice Center. Snow Watch 1980. *Glaciological Data, GD-11,* G. Kukla, A. Hecht, and D. Wiesnet, Eds., World Data Center A for Glaciology, 71–77.

Gorshkov, S. G., 1983: *World Ocean Atlas. Volume 3: Arctic Ocean.* Department of Navigation and Oceanography, Ministry of Defense, USSR, Pergamon Press, 184 pp.

Grenfell, T. C., and G. A. Maykut, 1977: The optical properties of ice and snow in the Arctic Basin. *J. Glaciol.*, **80,** 445–463.

——, and D. K. Perovich, 1984: Spectral albedos of sea ice and incident solar irradiance in the southern Beaufort Sea. *J. Geophys. Res.*, **89,** 3573–3580.

——, and A. W. Lohanick, 1985: Temporal variations of the microwave signatures of sea ice during the late spring and early summer near Mould Bay, NWT. *J. Geophys. Res.*, **90,** 5063–5074.

Hansen, J., D. Johnson, A. Lacis, P. Lebedeff, D. Lee, D. Rind, and G. Russell, 1983: Climatic effects of atmospheric carbon dioxide. *Science,* **220,** 873–875.

Hanson, A. M., 1980: The snow cover of sea ice during the Arctic Ice Dynamics Joint Experiment, 1975 to 1976. *Arc. Alp. Res.*, **12,** 215–226.

Hanson, K. J., 1961: The albedo of sea-ice and ice islands in the Arctic Ocean basin. *Arctic,* **14,** 188–196.

Herman, G., and R. Goody, 1976: Formation and persistence of Arctic stratus clouds. *J. Atmos. Sci.*, **33,** 1537–1553.

Hibler, W. D., III, 1979: A dynamic thermodynamic sea ice model. *J. Phys. Oceanogr.*, **9,** 815–846.

Holmgren, G., C. Benson, and G. Weller, 1975: A study of the breakup of the Arctic slope of Alaska by ground, air and satellite observations. *Climate of the Arctic,* G. Weller and S. A. Bowling, Eds., 24th Alaska Science Conf., 358–366.

Holt, G., and S. A. Digby, 1985: Processes and imagery of first-year fast sea ice during the melt season. *J. Geophys. Res.*, **90,** 5045–5062.

Hummel, J. R., and R. A. Reck, 1979: A global surface albedo model. *J. Appl. Meteor.*, **18,** 239–253.

Huschke, R. E., 1969: Arctic cloud statistics from "air calibrated" surface weather observations. United States Air Force Project Rand Contract F44620-67-C-0015, 79 pp.

Jacobs, J. D., R. G. Barry, and R. L. Weaver, 1975: Fast ice characteristics, with special reference to the eastern Canadian Arctic. *Polar Record,* **17,** 521–536.

Key, J., and R. G. Barry, 1989: Cloud cover analysis with Arctic AVHRR data, 1. Cloud detection. *J. Geophys. Res.*, **94,** 18 521–18 535.

——, and S. Peckham, 1991: Probable errors in width distributions of sea ice leads measured along a transect. *J. Geophys. Res.*, **96**(C10), 18 417–18 423.

Kukla, G., and D. A. Robinson, 1980: Annual cycle of surface albedo. *Mon. Wea. Rev.*, **108,** 56–68.

——, and ——, 1988: Variability of summer cloudiness in the Arctic Basin. *Meteor. Atmos. Phys.*, **39,** 42–50.

Kuznetsov, I. M., and A. A. Timerev, 1973: The dependence of ice albedo changes on the ice cover state as determined by airborne observations. *Problems of the Arctic and Antarctic,* **40,** 67–74.

Laktionov, A. F., Ed., 1953: *Rukovodstvo dlya nablyudeniy nad l'dami arkticheskikh morey, rek i ozer na polyarnykh gidrometeorologicheskikh stantsiyakh* (Handbook for observing the ice of Arctic seas, rivers and lakes at polar hydrometeorological stations), Izdatel'stvo Glavsevmorputi, Leningrad (Serii Posobiya Rukovodstva, 31).

Langleben, M. P., 1971: Albedo of melting sea ice in the southern Beaufort Sea. *J. Glaciol.*, **10,** 101–104.

Lapp, D., 1982: *A Study of Ice Meltponds.* Atmos. Envir. Ser., Envir. Canada, 62 pp.

Larsson, P., and S. Orvig, 1962: *Albedo of Arctic Surfaces.* Publ. in Meteor. No. 54, McGill University, Montreal, 41 pp.

Marshunova, M. S., and N. T. Chernigovskiy, 1966: Numerical characteristics of the radiation regime in the Soviet Arctic. *Proc. Symp. Arctic Heat Budget and Atmospheric Circulation,* J. O. Fletcher, Ed., Memo. RM-5233-NSF, Rand Corp, 279–297.

——, and ——, 1978: *Radiation Regime of the Foreign Arctic.* Gid-

rometeoizdat, Leningrad, Natl. Sci. Found. Tech. Translation 72-51034, 189.

Maykut, G. A., 1982: Large-scale heat exchange and ice production in the central Arctic. *J. Geophys. Res.*, **87**(C10), 7971–7984.

——, 1986: Surface heat and mass balance. *The Geophysics of Sea Ice,* N. Untersteiner, Ed., (NATO ASI Series, Series B, Physics, vol 146), Plenum Press, 395–463.

Morassutti, M., 1989: *Climate Model Sensitivity to Sea Ice Albedo Parameterization.* M.A. thesis, Dept. of Geography, University of Colorado, Boulder, 151 pp.

Nazintsev, Y. L., 1964: Teplovoy balans poverkhnosti mnogoletnego ledyanogo pokrova v tsentral'noy Arktike (Surface heat balance of the perennial ice sheet of the central Arctic). *Tr. Arkt. Antark. Nauchno Issled. Inst.*, **267,** 110–126.

Pautzke, C. G., and G. F. Hornof, 1978: Radiation regime during AIDJEX: A data report. *AIDJEX Bull.*, **39,** 165–185.

Payne, R. E., 1972: Albedo of the sea surface. *J. Atmos. Sci.*, **29,** 959–970.

Posey, J. W., and P. F. Clapp, 1964: Global distribution of normal surface albedo. *Geofis. Inter.*, **4,** 33–48.

Preuss, H. J., and J. F. Geleyn, 1980: Surface albedos derived from satellite data and their impact on forecast models. *Arch. Meteor. Geophys. Bioclim.*, **A29,** 345–356.

Robinson, D. A., 1986: Initiation of spring snowmelt over Arctic lands. *Cold Regions Hydrology Symp.*, Amer. Water Resources Assoc., 547–554.

——, and G. Kukla, 1985: Maximum surface albedo of seasonally snow-covered lands in the Northern Hemisphere. *J. Clim. Appl. Meteor.*, **24,** 402–411.

——, G. J. Kukla, and M. C. Serreze, 1985: Arctic Cloud Cover during the Summers of 1977–1979. Lamont–Doherty Geological Observatory Tech. Rep. L-DGO-85-5, 175 pp.

——, G. Scharfen, M. C. Serreze, G. Kukla, and R. G. Barry, 1986: Snow melt and surface albedo in the Arctic basin. *Geophys. Res. Lett.*, **13,** 945–948.

——, ——, R. G. Barry, and G. Kukla, 1987: Analysis of interannual variations of snow melt on Arctic sea ice mapped from meteorological satellite imagery. *Large Scale Effects of Seasonal Snow Cover. Proc. of the Vancouver Symp.*, B. Goodison and R. G. Barry, Eds., 315–327.

Robock, A., 1980: The seasonal cycle of snow cover, sea ice and surface albedo. *Mon. Wea. Rev.*, **108,** 267–285.

Ross, B., and J. E. Walsh, 1987: A comparison of simulated and observed fluctuations in summertime Arctic surface albedo. *J. Geophys. Res.*, **92,** 13 115–13 125.

Rossow, W. B., C. L. Brest, and L. C. Gardner, 1989: Global, seasonal surface variations from satellite radiance measurements. *J. Climate,* **2,** 214–247.

Scharfen, G., R. G. Barry, D. A. Robinson, G. Kukla, and M. C. Serreze, 1987: Large-scale patterns of snow melt on Arctic sea ice mapped from meteorological satellite imagery. *Ann. Glaciol.*, **9,** 1–6.

Serreze, M. C., and R. G. Barry, 1988: Synoptic activity in the Arctic Basin, 1979–85. *J. Climate,* **1,** 1276–1295.

——, and M. C. Rehder, 1990: June cloud cover over the Arctic Ocean. *Geophys. Res. Lett.*, **17,** 2397–2400.

——, J. A. Maslanik, R. H. Preller, and R. G. Barry, 1990: Sea ice concentrations in the Canada Basin during 1988: Comparisons with other years and evidence of multiple forcing mechanisms. *J. Geophys. Res.*, **95,** 22 253–22 267.

Shine, K. P., and A. Henderson-Sellers, 1984: Cryosphere-cloud interactions near the snow/ice limit: Sensitivity testing of model parameterizations. *Cryosphere-Cloud Interactions near the Snow/Ice Limit,* A. Henderson-Sellers and R. G. Barry, Eds., University of Colorado, CIRES and Department of Geography, University of Liverpool, 77–236.

Taylor, B. R., and L. L. Stowe, 1984: Reflectance characteristics of uniform earth and cloud surfaces derived from NIMBUS-7 ERB. *J. Geophys. Res.*, **89,** 4987–4996.

Thorndike, A. S., and R. Colony, 1980: *Arctic Ocean Buoy Program Data Report, 1 January 1979–31 December, 1979.* Polar Science Center, University of Washington, Seattle, 127 pp.

Untersteiner, N., 1961: On the mass and heat budget of Arctic sea ice. *Arch. Meteor., Geophys., Bioclim.*, **12,** 151–182.

Wen, T., G. R. Barrison, and R. E. Francois, 1980: Melt season changes in Arctic ice. *Int. Forum Ocean Engineering in the '80s, Proc. Oceans '80s,* IEEE, 114–122.

Zubov, N. N., 1963: *L'dy Arktiki.* Izdatel'stvo Glavsevmorputi, Moscow, 1945, Translation: *Arctic Ice,* U.S. Navy Oceanographic Office, 491 pp.